Materials Science in Semiconductor Processing 180 (2024) 108539

Contents lists available at ScienceDirect

Materials Science in Semiconductor Processing

journal homepage: www.elsevier.com/locate/mssp

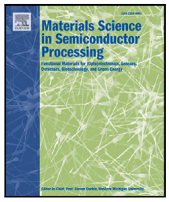

3D finite-element modeling of topological photonics in germanium

Ian Colombo, Jacopo Pedrini *, Eliseo Iemmolo, Fabio Pezzoli

Dipartimento di Scienza dei Materiali, Università degli Studi di Milano-Bicocca and BiQuTe, via R. Cozzi 55, Milan, 20125, (MI), Italy

ARTICLE INFO

Keywords:
Photonic crystals
Topological photonics
Chiral optics
Silicon photonics
Germanium
Heterostructures

ABSTRACT

We investigated the photonic properties of topological lattices specifically designed to open a terahertz photonic bandgap in a germanium matrix. An extensive analysis based on three-dimensional finite element method enabled the identification of the requirements in terms of vertical height and lateral dimensions of the Ge motifs to suitably vary the bulk gap between 41 and 65 THz. Furthermore, by interfacing topologically distinct domains, we were able to observe the emergence of non-trivial edge modes that remain stable at a constant frequency despite the varying geometry of the unit cells. These findings provide valuable insights for designing resilient and effective photonic devices based on topological photonic crystals, and open new avenues for the realization of advanced quantum technologies in the THz regime.

1. Introduction

Recent years have seen a huge increase in interest in topological photonic crystals (TPCs) because they provide a convenient photonic analogue that mimic the behavior of electrons in condensed matter. This is because TPCs allow for the reproduction of exotic physics observed in topological insulators, with a high degree of customization and control over the various degrees of freedom that characterize a system [1,2]. TPCs have exceptional characteristics, such as chiral and unidirectional light propagation [3], resistance to abrupt bends [4], and mathematical protection against defect-induced scattering. These properties open the door for the construction of efficient photonic circuits [5,6] based on topological components such as filters [7], resonators [8], waveguides [3,9,10], and lasers [9,11,12]. Yet, there have been challenges in TPC advancement, particularly with regard to the operation in the terahertz (THz) spectral range. This frequency region is strategic because it offers large bandwidth for high-frequency data transmission, an essential component for improving communication networks beyond current limitations [13,14]. Other crucial applications of THz waves include security, biological sensing, non-destructive imaging, and quantum information [13–15]. TPCs based on Ge hold the promise to spark the development of efficient THz photonic components and devices [16]. 3D Ge lattices, such as those schematically shown in Fig. 1a can be easily obtained through top-down fabrication of well-established Ge-on-Si heterostructures or through direct epitaxial self-assembly [17–19]. Photonic crystals based on the Ge-on-insulator variant are also available. Such lattices of Ge blocks are suitable candidates for the investigation of unique photonic and topological features as they bear in-plane resemblance to typical square TPCs studied in other materials and frequency range [11,20–24].

In this work we examined the electromagnetic wave confinement in a 3-dimensional environment by taking advantage of finite element analysis. By addressing realistic designs we were able to introduce robust and effective photonic devices based on THz TPCs. The simple extension of the topological lattices in the third dimension, while maintaining the ease of fabrication, introduces an additional degree of freedom for controlling the magnitude of the photonic bandgap (PBG) and its frequency range and is also needed for establishing a Ge crystal critical height above which the topological modes disappear.

2. Calculation details

In this work, FEM calculations were based on the unit cell presenting a Ge block in its center, surrounded by vacuum. To provide data that may be experimentally accessible, the shape of the Ge micropillars was chosen in agreement with already established manufacturing processes of such heteroepitaxial microstructures [18], with a pseudo-octagonal shape presenting both {100} and {111} facets. The unit cell is depicted in Fig. 1b, with a defined lattice parameter of $a = 2$ μm and the Ge micropillar in the center with a lateral size parameter d and the size of the {111} facet of $0.1d$. The real part of the refractive index is $n = 4$ for Ge [25] that is assumed to be constant in the spectral range of tens of THz, and $n = 1$ for vacuum, while the extinction coefficient is zero. The 3D simulation was performed by changing the parameter h that indicates the size of the micropillar along the growth axis, *i.e.* in the z direction (see Fig. 1a). Since dedicated calculations (not shown) demonstrated that the insertion of the underlying Si pillars do not affect the results, in the following we will simplify the lattice geometry by considering only the Ge crystals. Furthermore, since the Si pillar has sub-wavelength dimensions, we

* Corresponding author.
E-mail address: jacopo.pedrini@unimib.it (J. Pedrini).

https://doi.org/10.1016/j.mssp.2024.108539
Received 29 February 2024; Received in revised form 11 May 2024; Accepted 14 May 2024

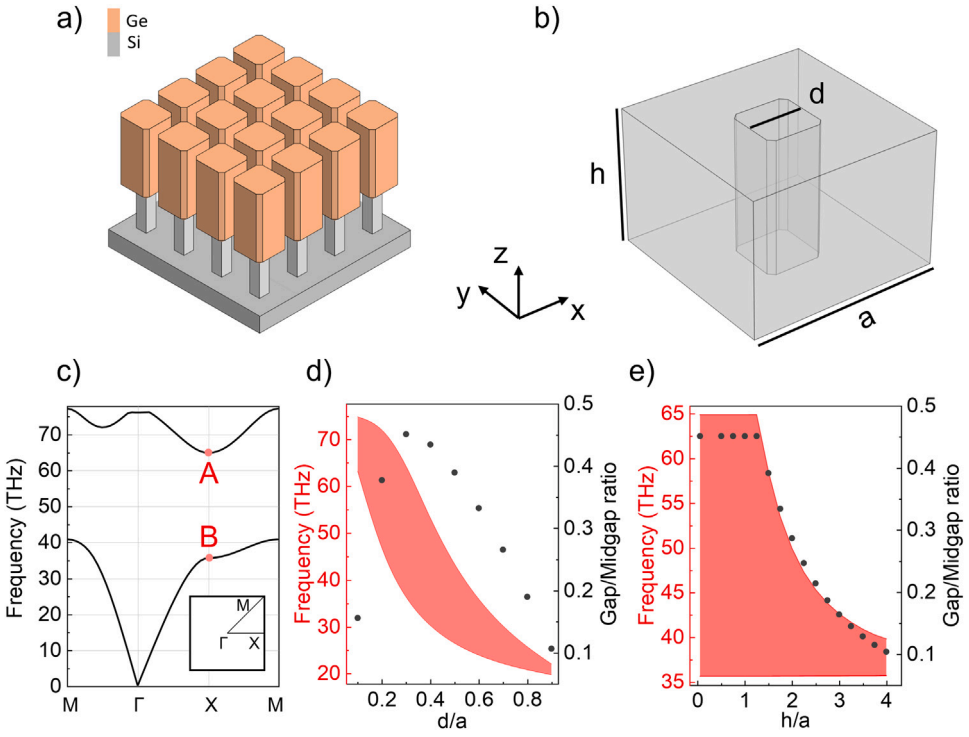

Fig. 1. (a) Graphical representation of the photonic crystal based on a Ge (orange) on Si (gray) heterostructure (not to scale). (b) PC's fundamental unit structure model with lattice parameter $a = 2$ μm and height $h = 1.4$ μm, composed of a central Ge pillar with refractive index $n = 4$ and $0.1d$ chamfers at the four corners, surrounded by vacuum with refractive index $n = 1$. (c) Dispersion diagram for the unit cell with $d/a = 0.3$ obtained by finite element analysis. (d) PBG calculated in the X point of the bandstructure (red area) and gap/midgap ratio (black dots) as a function of the aspect ratio d/a. (e) Evaluation of the PBG size at the X point (red area) and gap/midgap ratio (black dots), in relation to the size of the Ge pillar.

did not account for potential significant substrate losses. Nonetheless, a more in-depth analysis of losses associated with the specific production technology chosen is required. Later in the text, certain strategies to tolerate losses already available in the literature are mentioned. The computational analysis of the system eigenfrequencies was performed with Comsol Multiphysics [26], using periodic Floquet boundary conditions to evaluate the photonic bandstructure when the system had an in-plane 2D periodicity. The Floquet boundary conditions are helpful in FEM simulations because of the restrictions on the electromagnetic field at the unit cell's boundaries, making the latter reflectionless while guaranteeing momentum and energy conservation. This, in turn, allows the study of periodic structures at a lower computational cost.

2.1. Unit cell calculations

Within the irreducible Brillouin Zone (IBZ), we systematically swept the wavevector k along high-symmetry directions, as shown in the inset of Fig. 1c. The magnitude of the PBG depends on the size of the elements composing the unit cell [16]. Therefore, we calculated the photonic bandstructure as a function of the micropillar lateral size d, this allowed us to find the dimensions of the Ge micropillar that maximize the magnitude of the PBG. An example of the photonic bandstructure is reported in Fig. 1c, for $d = 0.3a$. The bandstructure presents a full PBG centered at about 50 THz and ~30 THz wide. The eigenfrequency analysis allows us to evaluate the frequency position and bandwidth of the PBG at X, as reported in Fig. 1d. The significance of these evaluations at such high symmetry point is required for the topological mode to emerge and will be discussed later. Since both the frequency position and the extension of the PBG depend on the size of the micropillar [27], we renormalized the extension of the bandgap to its mid-gap frequency. Fig. 1d shows that the gap opens when initially increasing the size of the micropillar, and then it rapidly shrinks in size, almost closing for $d = 0.9a$. The maximum value of the PBG is achieved when $d = 0.3a$. In the following, this value will be set as the fixed micropillar lateral size.

After having defined the optimal lateral size to obtain the largest PBG, we carried out a study as a function of the unit cell in the out-of-plane direction, i.e., z, by varying the parameter h, and evaluating the frequency value and the width of the PBG at the X point. The results are summarized in Fig. 1e. Initially, the PBG is large and constant despite the thickness of the micropillar is increased up to $h = 1.25a$. Above this critical value the bandgap quickly collapses since the top-band rapidly decreases in energy. It should be noted, however, that a PBG is still observed for a thickness as large as $h = 4a$.

Having discussed the band structure of the Ge photonic crystal and how it depends on the unit cell parameters, we now show how we can leverage its topological properties. As illustrated in Fig. 2a, we identify two lattices that can be viewed as the photonic analogues of the 2D Su–Schrieffer–Heeger (SSH) model [20,28,29]. Highlighted with the red dashed line is the unit cell of the structure described before (*compressed*), and the second one, where a unit cell is made up of four elements equally spaced from the cell's center, is highlighted with the blue solid line (*expanded*). We specifically studied the out-of-plane electric field E_z distribution, which is shown for such unit cells in Fig. 2b. In this case, the *compressed* PC exhibits an odd distribution in the high-energy band and an even E_z distribution in the lower band. In the *expanded* structure, the contrary holds true. The symmetry of the eigenfunctions is different because they have opposite parity, but the band structure of the two lattices is the same as in the SSH model, where the band dispersion does not change with the inversion of the intra- and inter-cellular distances between the elements composing the unit cell [20,29]. As a result, the parity of the bands can be considered as the topological invariant so that the *compressed* and *expanded* PCs belong to different topological phases.

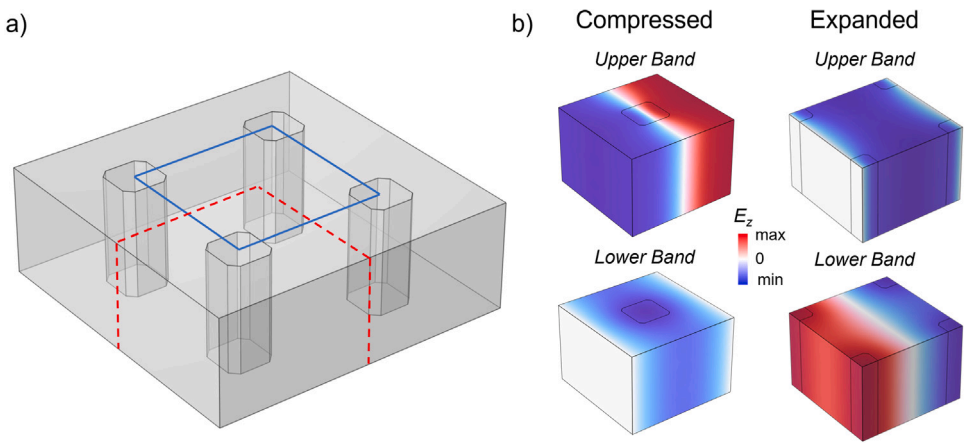

Fig. 2. (a) Visualization of the *compressed* (red dashed line) and *expanded* (blue solid line) unit cells. (b) Distribution of the electric field for both compressed and expanded PCs for $d/a = 0.3$. The upper and lower band are points A and B in Fig. 1c, respectively. Out-of-plane electric field E_z component at the X-point of the irreducible Brillouin zone. A topological phase transition is suggested by the symmetry inversion between the compressed and expanded crystal shapes.

2.2. Supercell calculations

A fingerprint of the occurrence of TPCs is the presence of localized modes at the interface between domains characterized by different topology. To verify this property, we simulated a ribbon composed of the two PCs described in Fig. 2b that are placed in contact, in a configuration commonly referred to as a *supercell*, as seen in Fig. 3a. For the simulation, we used Floquet periodic boundary conditions only along the x direction. This structure is a one-dimensional photonic crystal and therefore its eigenfrequencies were calculated from $k_x = 0$ to $k_x = \frac{\pi}{a}$. The calculated bandstructure of such supercell is shown in Fig. 3b, for the Ge micropillar thickness $h = 0.75a$. It exhibits a wide range of bulk modes with a PBG spanning from 41 to 65 THz, and one well-separated, localized mode centered at about 42.5 THz, highlighting the topological nature of the designed interface. This mode is not only well-defined in energy, but the E_z plot in Fig. 3a illustrates its spatial localization at the interface between the two domains, providing evidence of the existence of a topological transition in the designed supercell [9,30–33]. Fig. 3a also represents the local Poynting vectors, which show the direction of propagation of the electromagnetic wave. We then investigated the evolution of the photonic bandstructure and of the topological mode as a function of the micropillar thickness h. As shown in Fig. 3c-d, we evaluated the PBG at the critical points $k_x = 0$ and $k_x = \pi/a$, reporting the frequency position of the topological mode and the extension of the PBG. As already observed for the unit cell, it can be clearly seen that for both values of k_x the PBG is initially almost constant with increasing h, and then it rapidly shrinks due to a fast decrease of the high-energy band. The value at which the PBG starts to shrink is different between the two scenarios: it is $h = a$ for the calculation performed in $k_x = 0$ and $h = 1.25a$ for that performed in $k_x = \pi/a$.

After having analyzed the size of the bandgap as a function of h we focus on the behavior of the topological mode. Fig. 3c-d show that in both points of the bandstructure of the supercell, the topological mode remains robust and at constant energy. When the high-energy band crosses the energy at which the topological mode can be found, the latter disappears into the bulk. This happens for $h = 1.5a$ in $k_x = 0$ and for $h = 2a$ in $kx = \pi/a$. Therefore, to preserve the presence of the topological mode at the interface between the two PC domains, future fabrication efforts will require careful consideration of the aspect ratio of the 3D crystal. In our case study we were able to set an upper value for the Ge micropillars of $h = 1.5a$. Modern lithography achieves submicrometer resolutions, while epitaxial Ge crystal self-assembly offers control down to single monolayer levels. Spatial errors in height and lattice parameters result in a manageable relative error for the h/a ratio, as observed in Fig. 3c-d, without compromising the topological state. In addition, by directly integrating these photonic crystal structures onto 3D structured silicon-on-insulator (SOI) substrates, the suggested fabrication methods can minimize substrate losses caused by the large refractive index difference [34].

3. Conclusion

Our goal to extend our calculation to 3D was pivotal for understanding the complex behavior of Ge micropillars in the context of the topological mode in the THz frequency range. To guarantee the presence of the topological mode, we specifically found that the maximum height for micropillars is $h = 1.5a$. This offers insightful information about the design parameters and opens the way to the fabrication of Ge-based THz TPCs that are robust and efficient.

CRediT authorship contribution statement

Ian Colombo: Visualization, Formal analysis, Data curation. **Jacopo Pedrini:** Writing – review & editing, Supervision. **Eliseo Iemmolo:** Data curation. **Fabio Pezzoli:** Writing – review & editing, Validation, Supervision, Funding acquisition, Conceptualization.

Declaration of competing interest

The authors declare the following financial interests/personal relationships which may be considered as potential competing interests: Fabio Pezzoli reports financial support was provided by Horizon Europe. Jacopo Pedrini reports financial support was provided by European Social Fund. If there are other authors, they declare that they have no known competing financial interests or personal relationships that could have appeared to influence the work reported in this paper.

Data availability

Data will be made available on request.

Acknowledgments

The authors thank P. Minazzi for the scientific discussions. This work has been funded by the European Union's Horizon Europe Research and Innovation Programme under agreement 101070700. J.P. acknowledges financial support from FSE REACT-EU (grant 2021-RTDAPON-144).

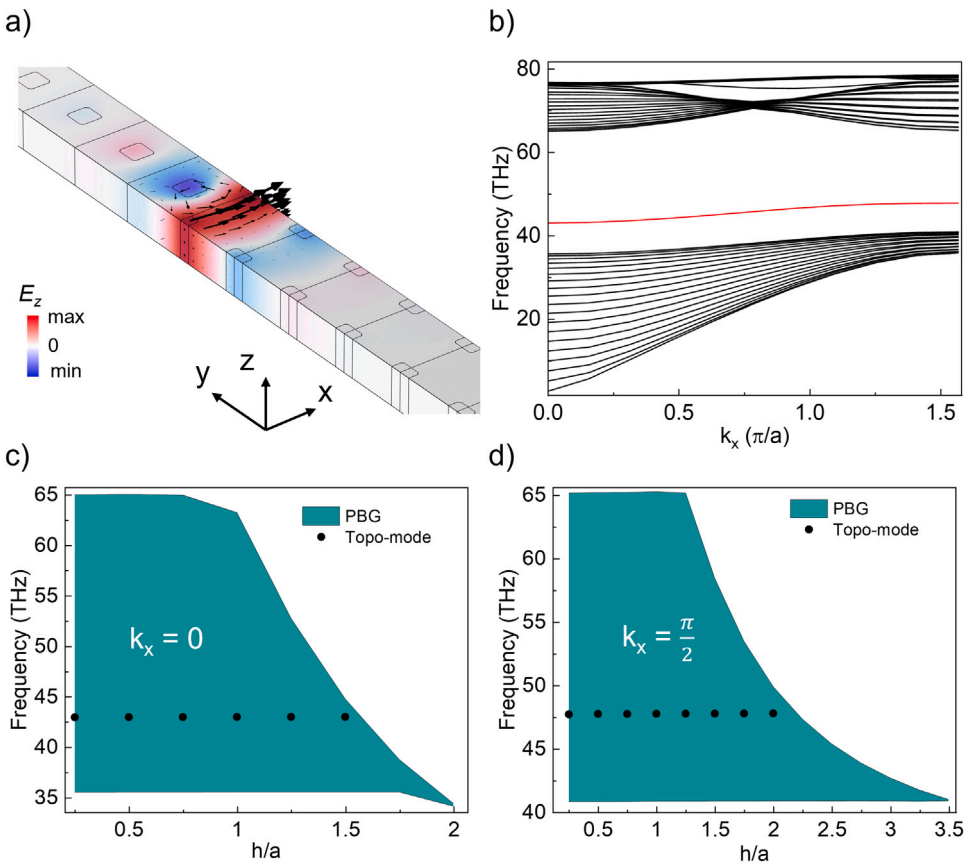

Fig. 3. (a) Spatial distribution of the out-of-plane component of the electromagnetic field (E_z) in a supercell configuration, consisting of a line interface between a compressed and expanded PC. The Poynting vector's direction and magnitude are indicated by black arrows. ($h = 0.75a$) (b) Calculated bandstructure of the supercell along the x direction. Bulk bands (gray) and a gap containing a localized topological mode (red curve) are visible in the bandstructure. The interface between the two PC zones is where the modes are limited. ($h = 0.75a$) (c,d) PBG and topological mode frequency dependence in relation to the height of the unit cell, in Γ (left) and in X (right).

References

[1] M.Z. Hasan, C.L. Kane, Colloquium: Topological insulators, Rev. Modern Phys. 82 (4) (2010) 3045–3067, http://dx.doi.org/10.1103/RevModPhys.82.3045.

[2] T. Ozawa, H.M. Price, A. Amo, N. Goldman, M. Hafezi, L. Lu, M.C. Rechtsman, D. Schuster, J. Simon, O. Zilberberg, I. Carusotto, Topological photonics, Rev. Modern Phys. 91 (2019) 015006, http://dx.doi.org/10.1103/RevModPhys.91.015006.

[3] N. Parappurath, F. Alpeggiani, L. Kuipers, E. Verhagen, Direct observation of topological edge states in silicon photonic crystals: Spin, dispersion, and chiral routing, Sci. Adv. 6 (10) (2020) eaaw4137, http://dx.doi.org/10.1126/sciadv.aaw4137.

[4] J.-K. Yang, Y. Hwang, S.S. Oh, Evolution of topological edge modes from honeycomb photonic crystals to triangular-lattice photonic crystals, Phys. Rev. Res. 3 (2021) L022025, http://dx.doi.org/10.1103/PhysRevResearch.3.L022025.

[5] J.W. Dong, X.D. Chen, H. Zhu, Y. Wang, X. Zhang, Valley photonic crystals for control of spin and topology, Nature Mater. 16 (3) (2017) 298–302, http://dx.doi.org/10.1038/nmat4807.

[6] P. Lodahl, S. Mahmoodian, S. Stobbe, A. Rauschenbeutel, P. Schneeweiss, J. Volz, H. Pichler, P. Zoller, Chiral quantum optics, Nature 541 (7638) (2017) 473–480, http://dx.doi.org/10.1038/nature21037, arXiv:1608.00446.

[7] M.J. Mehrabad, A.P. Foster, N.J. Martin, R. Dost, E. Clarke, P.K. Patil, M.S. Skolnick, L.R. Wilson, Chiral topological add–drop filter for integrated quantum photonic circuits, Optica 10 (3) (2023) 415–421, http://dx.doi.org/10.1364/OPTICA.481684.

[8] M. Jalali Mehrabad, A.P. Foster, R. Dost, E. Clarke, P.K. Patil, I. Farrer, J. Heffernan, M.S. Skolnick, L.R. Wilson, A semiconductor topological photonic ring resonator, Appl. Phys. Lett. 116 (6) (2020) 061102, http://dx.doi.org/10.1063/1.5131846.

[9] Y. Zeng, U. Chattopadhyay, B. Zhu, B. Qiang, J. Li, Y. Jin, L. Li, A.G. Davies, E.H. Linfield, B. Zhang, Y. Chong, Q.J. Wang, Electrically pumped topological laser with valley edge modes, Nature 578 (7794) (2020) 246–250, http://dx.doi.org/10.1038/s41586-020-1981-x.

[10] M. Jalali Mehrabad, A.P. Foster, R. Dost, E. Clarke, P.K. Patil, A.M. Fox, M.S. Skolnick, L.R. Wilson, Chiral topological photonics with an embedded quantum emitter, Optica 7 (12) (2020) 1690, http://dx.doi.org/10.1364/OPTICA.393035.

[11] C. Han, M. Kang, H. Jeon, Lasing at multidimensional topological states in a two-dimensional photonic crystal structure, ACS Photonics 7 (8) (2020) 2027–2036, http://dx.doi.org/10.1021/acsphotonics.0c00357.

[12] Y. Ota, R. Katsumi, K. Watanabe, S. Iwamoto, Y. Arakawa, Topological photonic crystal nanocavity laser, Commun. Phys. 1 (1) (2018) 4–6, http://dx.doi.org/10.1038/s42005-018-0083-7, arXiv:1806.09826.

[13] Y. Yang, Y. Yamagami, X. Yu, P. Pitchappa, J. Webber, B. Zhang, M. Fujita, T. Nagatsuma, R. Singh, Terahertz topological photonics for on-chip communication, Nature Photonics 14 (7) (2020) 446–451, http://dx.doi.org/10.1038/s41566-020-0618-9, arXiv:1904.04213.

[14] A. Kumar, M. Gupta, P. Pitchappa, N. Wang, M. Fujita, R. Singh, Terahertz topological photonic integrated circuits for 6G and beyond: A perspective, J. Appl. Phys. 132 (14) (2022) 140901, http://dx.doi.org/10.1063/5.0099423.

[15] A. Leitenstorfer, A.S. Moskalenko, T. Kampfrath, J. Kono, E. Castro-Camus, K. Peng, N. Qureshi, D. Turchinovich, K. Tanaka, A.G. Markelz, M. Havenith, C. Hough, H.J. Joyce, W.J. Padilla, B. Zhou, K.-Y. Kim, X.-C. Zhang, P.U. Jepsen, S. Dhillon, M. Vitiello, E. Linfield, A.G. Davies, M.C. Hoffmann, R. Lewis, M. Tonouchi, P. Klarskov, T.S. Seifert, Y.A. Gerasimenko, D. Mihailovic, R. Huber, J.L. Boland, O. Mitrofanov, P. Dean, B.N. Ellison, P.G. Huggard, S.P. Rea, C. Walker, D.T. Leisawitz, J.R. Gao, C. Li, Q. Chen, G. Valušis, V.P. Wallace, E. Pickwell-MacPherson, X. Shang, J. Hesler, N. Ridler, C.C. Renaud, I. Kallfass, T. Nagatsuma, J.A. Zeitler, D. Arnone, M.B. Johnston, J. Cunningham, The 2023 terahertz science and technology roadmap, J. Phys. D: Appl. Phys. 56 (22) (2023) 223001, http://dx.doi.org/10.1088/1361-6463/acbe4c.

[16] I. Colombo, P. Minazzi, E. Bonera, F. Pezzoli, J. Pedrini, THz higher-order topological photonics in Ge-on-Si heterostructures, 2024, arXiv:2402.15622.

[17] J. Pedrini, P. Biagioni, A. Ballabio, A. Barzaghi, M. Bonzi, E. Bonera, G. Isella, F. Pezzoli, Broadband control of the optical properties of semiconductors through site-controlled self-assembly of microcrystals, Opt. Express 28 (17) (2020) 24981, http://dx.doi.org/10.1364/oe.398098.

[18] J. Pedrini, A. Barzaghi, J. Valente, D.J. Paul, G. Isella, F. Pezzoli, Photonic band gap and light routing in self-assembled lattices of epitaxial Ge -on-Si microstructures, Phys. Rev. A 16 (6) (2021) 1, http://dx.doi.org/10.1103/PhysRevApplied.16.064024.

[19] V. Falcone, A. Ballabio, A. Barzaghi, C. Zucchetti, L. Anzi, F. Bottegoni, J. Frigerio, R. Sordan, P. Biagioni, G. Isella, Graphene/Ge microcrystal photodetectors with enhanced infrared responsivity, APL Photonics 7 (4) (2022) http://dx.doi.org/10.1063/5.0082421, 046106.

[20] B.Y. Xie, G.X. Su, H.F. Wang, H. Su, X.P. Shen, P. Zhan, M.H. Lu, Z.L. Wang, Y.F. Chen, Visualization of higher-order topological insulating phases in two-dimensional dielectric photonic crystals, Phys. Rev. Lett. 122 (23) (2019) 233903, http://dx.doi.org/10.1103/PhysRevLett.122.233903.

[21] X.D. Chen, W.M. Deng, F.L. Shi, F.L. Zhao, M. Chen, J.W. Dong, Direct observation of corner states in second-order topological photonic crystal slabs, Phys. Rev. Lett. 122 (23) (2019) 233902, http://dx.doi.org/10.1103/PhysRevLett.122.233902.

[22] M. Makwana, R. Craster, S. Guenneau, Topological beam-splitting in photonic crystals, Opt. Express 27 (11) (2019) 16088–16102, http://dx.doi.org/10.1364/OE.27.016088.

[23] K.H. Kim, K.K. Om, Multiband photonic topological valley-hall edge modes and second-order corner states in square lattices, Adv. Opt. Mater. 9 (8) (2021) 1–7, http://dx.doi.org/10.1002/adom.202001865.

[24] Y.H. He, Y.F. Gao, H.Z. Lin, M.C. Jin, Y. He, X.F. Qi, Topological edge and corner states based on the transformation and combination of photonic crystals with square lattice, Opt. Commun. 512 (January) (2022) 128038, http://dx.doi.org/10.1016/j.optcom.2022.128038.

[25] T. Amotchkina, M. Trubetskov, D. Hahner, V. Pervak, Characterization of e-beam evaporated Ge, YbF3, ZnS, and LaF3 thin films for laser-oriented coatings, Appl. Opt. 59 (5) (2020) A40–A47, http://dx.doi.org/10.1364/AO.59.000A40.

[26] COMSOL multiphysics® v. 5.6., www.comsol.com. COMSOL AB, Stockholm, Sweden.

[27] J.D. Joannopoulos, Photonic Crystals: Molding the Flow of Light, second ed., Princeton University Press, 2008, http://dx.doi.org/10.2307/j.ctvcm4gz9.

[28] W.P. Su, J.R. Schrieffer, A.J. Heeger, Solitons in polyacetylene, Phys. Rev. Lett. 42 (25) (1979) 1698–1701, http://dx.doi.org/10.1103/PhysRevLett.42.1698.

[29] F. Liu, K. Wakabayashi, Novel topological phase with a zero berry curvature, Phys. Rev. Lett. 118 (7) (2017) 1–5, http://dx.doi.org/10.1103/PhysRevLett.118.076803.

[30] L.H. Wu, X. Hu, Scheme for achieving a topological photonic crystal by using dielectric material, Phys. Rev. Lett. 114 (22) (2015) 1–5, http://dx.doi.org/10.1103/PhysRevLett.114.223901.

[31] A.B. Khanikaev, G. Shvets, Two-dimensional topological photonics, Nature Photonics 11 (12) (2017) 763–773, http://dx.doi.org/10.1038/s41566-017-0048-5.

[32] Y. Gong, S. Wong, A.J. Bennett, D.L. Huffaker, S.S. Oh, Topological insulator laser using valley-hall photonic crystals, ACS Photonics 7 (8) (2020) 2089–2097, http://dx.doi.org/10.1021/acsphotonics.0c00521.

[33] M.I. Shalaev, W. Walasik, A. Tsukernik, Y. Xu, N.M. Litchinitser, Robust topologically protected transport in photonic crystals at telecommunication wavelengths, Nature Nanotechnol. 14 (1) (2019) 31–34, http://dx.doi.org/10.1038/s41565-018-0297-6.

[34] W.-J. Lee, H. Kim, J.-B. You, D.L. Huffaker, Ultracompact bottom-up photonic crystal lasers on silicon-on-insulator, Sci. Rep. 7 (1) (2017) 9543, http://dx.doi.org/10.1038/s41598-017-10031-8.